Article

A Novel 10-Watt-Level High-Power Microwave Rectifier with an Inverse Class-F Harmonic Network for Microwave Power Transmission

Jing Peng [1], Shouhao Wang [2],*, Xiaoning Li [3],* and Ke Wang [1]

[1]   Electric Power Science Research Institute, Yunnan Power Grid Co., Ltd., Kunming 650032, China; pengjing01@yn.csg.cn (J.P.); dkywangke@126.com (K.W.)
[2]   Electronic Information, University of Electronic Science and Technology of China, Chengdu 611731, China
[3]   Measuring and Testing Technologies and Instruments, University of Electronic Science and Technology of China, Chengdu 611731, China
*   Correspondence: shouhaowang@std.uestc.edu.cn (S.W.); lixn_uestc@uestc.edu.cn (X.L.)

Abstract: A novel 10-Watt-Level high-power microwave rectifier with an inverse Class-F harmonic network for microwave power transmission (MPT) is presented in this paper. The high-power microwave rectifier circuit comprises four sub-rectifier circuits, a 1×4 power divider, and a parallel-series dc synthesis network. The simple inverse Class-F harmonic control network serves dual roles: harmonic control and impedance matching. The 1×4 power divider increases the RF input power fourfold, reaching 40 dBm (10 W). The parallel-series dc synthesis network enhances the resistance to load variation. The high-power rectifier circuit is simulated, fabricated, and measured. The measurement results demonstrate that the rectifier circuit can reach a maximum RF input power of 10 W at 2.45 GHz, with a maximum rectifier efficiency of 61.1% and an output dc voltage of 23.9 V, which has a large application potential in MPT.

Keywords: microwave rectifier; high power; inverse Class-F; microwave power transmission (MPT)

1. Introduction

In recent years, the continuous development of new energy technology has resulted in an increased demand for cable-free charging and high-power charging solutions. As a research area within the field of wireless power transmission [1–3], MPT [4–7] represents a wireless charging system that transmits microwave energy for wireless charging. This technology offers the advantages of wireless charging, long-distance transmission [8,9], high power [10], and high flexibility [11], and it can be applied in a range of contexts [12], including smart factories, smart homes, smartphones, and new energy vehicles. Consequently, it has become a focus of increasing interest among scholars.

As a pivotal component within the MPT system, the microwave rectifier circuit serves to transform microwave energy received at the antenna end into direct current (dc) energy, thereby facilitating the charging of devices situated in its wake. The functionality of the microwave rectifier circuit is of paramount importance, as it directly influences the overall performance of the MPT system. Consequently, a comprehensive investigation of this circuit is essential for the advancement of microwave technology. The performance index of the rectifier circuit is reflected in a number of key areas [13], including high power [14,15], wide power [16,17], micro-power [18], wide bandwidth [19], wide load [20], small size [21], and so on. However, as society develops, there is a growing demand for high-power charging, particularly for smartphones and new energy vehicles. A high-power wireless charging system can significantly reduce charging times, enhancing convenience in people's lives. Therefore, it is essential to investigate the high-power performance index of the rectifier circuit.

The power capacity of a rectifier circuit is primarily contingent upon the reverse breakdown voltage (BV) of the core device diode [22]. When the diode's reverse BV is elevated, the rectifier circuit is capable of withstanding a greater input power. However, if the voltage at the ends of the diode surpasses the reverse BV, the diode will undergo a breakdown, rendering the rectifier circuit incapable of sustaining its functionality. To enhance the reverse BV of the diode, third-generation semiconductor technology can be employed to fabricate GaN Schottky diodes [23], which exhibit a high reverse BV. In paper [24], a GaN Schottky diode is employed to design a high-power microwave rectifier circuit, which exhibits a remarkably high reverse BV of 164 V, a low junction capacitance of 0.32 pF, and a low series resistance of 4.5 Ω, which are attributable to the sophisticated nature of the process. The 5.8 GHz high-power microwave rectifier circuit is designed based on a GaN Schottky diode and exhibits a maximum rectifier efficiency of 71% at an input power of 34 dBm, and its maximum input power can reach 38 dBm, which provides excellent performance. Nevertheless, this GaN Schottky diode has not been widely commercialized due to technological and economic constraints associated with the production process. Consequently, the most viable alternative is to utilize Si-based Schottky diodes with a comparatively lower reverse breakdown voltage, which are widely used commercially. In order to design high-power rectifier circuits using Si-based Schottky diodes, employing multiple diodes in series and parallel configurations or implementing a power divider network are viable solutions. In paper [25], an Si-based Schottky diode HSMS-282P is employed to design a high-power microwave rectifier circuit. The HSMS-282P (BV of per core = 15 V) comprises four series-parallel structured cores within the package, which significantly augment the power capacity of the diode with a single core. A high-power rectifier circuit with a doubled voltage structure based on the HSMS-282P has been designed. This circuit can reach 76% rectifier efficiency at an input power of 30 dBm and frequency of 433 MHz. A similar scheme is shown in paper [26] where four HSMS-282Ps are connected to realize the high-power rectifier, not only the series-parallel connection of the core but also the series-parallel connection of the diode, which greatly increase the input power capacity at 2.45 GHz. The measured maximum input power is 33 dBm and the rectifier efficiency is 66.8%. The series-parallel structure of papers [25,26] can indeed improve the power capacity of the rectifier circuit, but its power capacity is still not large enough. Therefore, we need to explore the use of other Si-based Schottky diodes with a higher reverse breakdown voltage in series and parallel to design a higher-power rectifier.

In this paper, a novel 10-Watt-Level high-power microwave rectifier with an inverse Class-F harmonic network for MPT is proposed. Firstly, a Si-based Schottky diode HSMS-270C (BV of per core = 25 V) with a high reverse breakdown voltage is selected. This diode is contained within a diode package chip comprising two cores, rather than the single core found in conventional chips HSMS-270B. This improvement in the number of cores within the chip allows for a doubling of the input power capacity of a single package chip. Secondly, this paper employs a remarkably simple structure for an inverse Class-F harmonic control network, comprising a section of short-circuited $\lambda/8$ microstrip line and a section of open-circuited $\lambda/12$ microstrip line. This configuration not only achieves harmonic control but also facilitates impedance matching, and four sub-rectifier circuits are designed based on an inverse Class-F harmonic network. Once more, this paper employs a 1×4 microstrip power divider to link four sub-rectifier circuits, enabling the RF input power to be multiplied by a factor of four (6 dB) and ultimately reaching a high-power input of 40 dBm (10 W). In conclusion, the dc synthesis method of parallel and then series at the output is employed to complete the dc power synthesis, thereby enhancing the rectifier circuits' resilience to load fluctuations and improving circuit stability. The 10 W class high-power rectifier circuit was simulated and designed using ADS 2020 software. The circuit was then cast for processing and actual testing, resulting in a 40 dBm (10 W) high-power input, 61.1% rectifier efficiency, 6.1 W dc output power, and 23.9 V dc output voltage at 2.45 GHz. In comparison to previous studies [23,24], the Si-based

diode utilized in this research is more readily available for purchase. Additionally, the total input power after incorporating the power divider and sub-rectifier is greater than that observed in the aforementioned studies. However, the BV value of a single GaN-based core is considerably larger than that of an Si-based core. Consequently, subsequent studies may wish to consider purchasing GaN diodes for rectifier circuit design. In comparison to the studies referenced [25,26], it can be observed that the single-core BV of the HSMS-270C diode utilized in this paper is larger than that of a HSMS-282P diode. Consequently, the rectifier circuits designed in this paper have a significantly enhanced input power compared to those in the aforementioned studies. In other words, this paper demonstrates a notable improvement in terms of power capacity.

## 2. Design of a High-Power Rectifier

The schematic of a novel 10W Level inverse Class-F high-power microwave rectifier circuit is illustrated in Figure 1. The rectifier circuit comprises three principal components: four sub-rectifier circuits, a 1×4 power divider, and parallel-series dc synthesis. Each sub-rectifier circuit comprises an inverse Class-F harmonic control network of $\lambda/8$ and $\lambda/12$ microstrip lines, a low-pass filter (Lout, Cout), an isolation capacitor (Cin), a Schottky diode HSMS-270C, and a resistor load (RL). A 1×4 microstrip power divider is employed at the center frequency point of 2.45 GHz. The parallel-serial dc synthesis structure is connected between the rectifier dc output and RL.
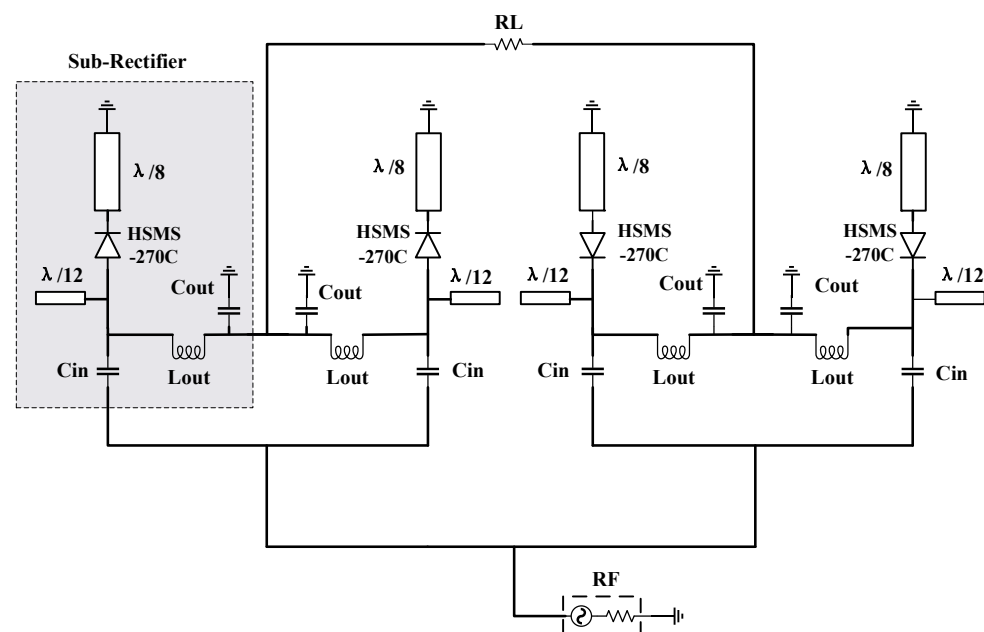
Figure 1. Schematic of the 10 W high-power rectifier.

2.1. Design of a Sub-Rectifier

This section presents the design of a single sub-rectifier circuit and illustrates its schematic in Figure 2a. The sub-rectifier is a 2.45 GHz sample inverse Class-F high-efficiency rectifier circuit with a shunt diode rectifier structure. It comprises the following main components: the circuit comprises a Schottky diode HSMS270C, an inverse Class-F harmonic control network, an LC low-pass filter (Lout, Cout), an isolation capacitor (Cin), and a resistor load (RL).
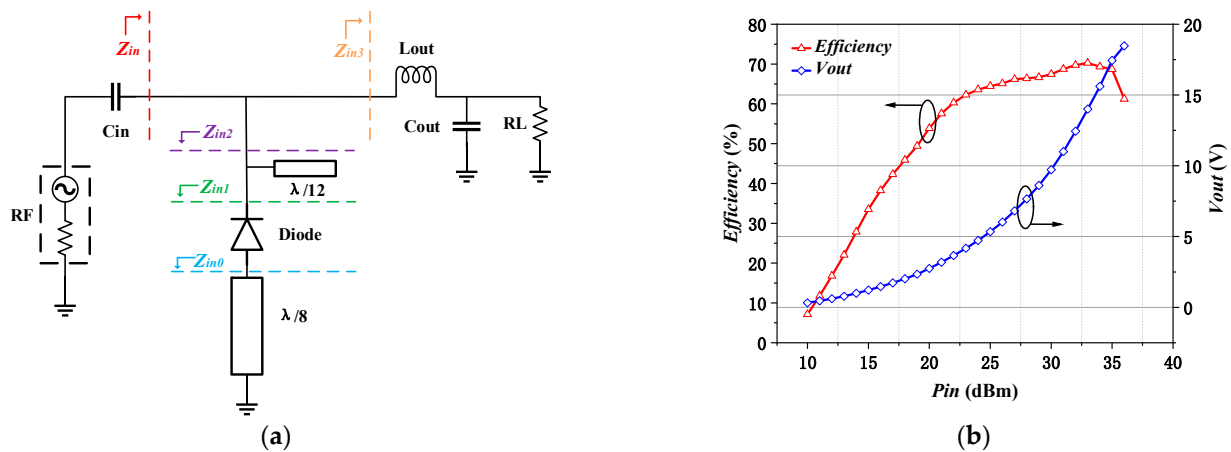
Figure 2. Design of the sub-rectifier: (**a**) schematic; (**b**) simulation of *efficiency* and *Vout* with *Pin*.

The inverse Class-F harmonic control network comprises two distinct sections: a $\lambda/8$ microstrip line and $\lambda/12$ microstrip line. This harmonic control network serves to reduce diode loss through waveform reshaping, while simultaneously reflecting the second and third harmonics back to the diode, thereby facilitating re-rectifier and enhancing rectifier efficiency. In accordance with the inverse Class-F harmonic impedance control theory [27–29], when all even harmonics exhibit high impedance and all odd harmonics exhibit low impedance, the voltage at both ends of the diode in the time domain manifests as a half-sinusoidal waveform; the current assumes the form of a square wave; and the diode's loss is zero when the voltage and current waveforms are completely staggered by 90 degrees. The ideal rectifier efficiency of the inverse Class-F is 100%. In consideration of the dimensions of the rectifier circuit and the insertion loss of the harmonic control network, it is sufficient to address the second and third harmonics. The $\lambda/8$ short microstrip line is connected in series between the diode and grounded, while the $\lambda/12$ open microstrip line is connected in parallel to the diode. From the input impedance calculation Formula (1), the impedance values of the $\lambda/8$ microstrip line and the $\lambda/12$ microstrip line at the fundamental frequency and its harmonics can be calculated. The impedance calculation formula is as follows (2) and (3): from the aforementioned equation, it can be observed that the $\lambda/8$ shorted microstrip line has a high impedance of ∞ at the second harmonic, while the $\lambda/12$ open microstrip line has a low impedance of 0 at the third harmonic. This outcome aligns with the harmonic control theory of the inverse Class-F.

$$Z_{in} = Z_0 \frac{Z_L + jZ_0 tan(\beta l)}{Z_0 + jZ_L tan(\beta l)} \tag{1}$$

$$Z_{\lambda/8}(\omega) = +jZ_8 tan\left(\frac{\pi}{4}\frac{\omega}{\omega_0}\right) = \begin{cases} jZ_8 & \omega = \omega_0 \\ \infty & \omega = 2\omega_0 \end{cases} \tag{2}$$

$$Z_{\lambda/12}(\omega) = -jZ_{12} cot\left(\frac{\pi}{4}\frac{\omega}{\omega_0}\right) = \begin{cases} -1.73jZ_{12} & \omega = \omega_0 \\ 0 & \omega = 3\omega_0 \end{cases} \tag{3}$$

The following section presents the derivation of the fundamental impedance matching process. The input impedance Z_{in0} of the $\lambda/8$ short microstrip line oriented inwards towards the grounded is (4) and can be considered to be equivalent to a series-connected inductor. The input impedance of the diode is $Z_{ind} = a - jb$, where a and b are unknown, and the input impedance Z_{in1} subsequent to the connection of both in series is (5). Furthermore, the parallel $\lambda/12$ open microstrip line fundamental impedance of $-1.73jZ_{12}$, which is equivalent to a parallel-connected capacitor, allows us to conclude that the entire parallel end of the input impedance Z_{in2} is (6). Furthermore, since the output LC low-pass filtering end of the fundamental is entirely filtered out, its input impedance can be equated to infinity ∞. Therefore, the input impedance Z_{in} of the whole sub-rectifier is Z_{in2} in (7). In

other words, the entire rectifier circuit input impedance Z_{in} can be considered equivalent to the parallel end of the input impedance Z_{in2}. In order to ensure that the rectifier circuit's input impedance is matched to 50 Ω, allowing the maximum possible RF signal to enter the rectifier, it is necessary to set Z_{in} = 50 Ω; the impedance matching of the whole sub-rectifier can be completed (8). In order to obtain the values of the four variables Z_8, Z_{12}, a, and b in (8), they can be analyzed in the following three steps: Firstly, the equivalent circuit model of the diode can be simulated in ADS to obtain the value of the diode input impedance $a - jb = 42 - j4\,\Omega$; consequently the values of $a = 42$ and $b = -4$ can be acquired. Secondly, the values of Z_8 and Z_{12} variables are unknown, and these two variables represent the characteristic impedance of $\lambda/8$ and $\lambda/12$ microstrip lines, respectively. When we first arbitrarily choose a section of the microstrip line's characteristic impedance to be fixed at a certain value, then the characteristic impedance of another microstrip line can be calculated. Ultimately, based on this premise, if Z_8 is initially established as 23 Ω, and $a = 42$ and $b = -4$ are known, Z_{12} can be calculated as 62.4 Ω. Thus, the fundamental impedance match theory of the rectifier circuit has been completely derived.

$$Z_{in0} = jZ_8 \tag{4}$$

$$Z_{in1} = Z_{in0} + Z_{ind} = a + j(Z_8 - b) \tag{5}$$

$$\begin{aligned}Z_{in2} &= Z_{in1} \parallel (-1.73\,jZ_{12}) \\ &= [a + j(Z_8 - b)] \parallel (-1.73jZ_{12})\end{aligned} \tag{6}$$

$$Z_{in} = Z_{in2} \parallel \infty = Z_{in2} \tag{7}$$

$$Z_{in} = [a + j(Z_8 - b)] \parallel (-1.73jZ_{12}) = 50 \tag{8}$$

The straight-through filtering at the conclusion of this section employs a capacitor and inductor to form a low-pass filter, which prevents the fundamental and harmonics from passing through the direct current (dc). The values of Lout and Cout are 51 nH and 68 pF, respectively. The RF input port is connected in series with a capacitor of 24 pF, which is designated as Cin. The use of capacitor Cin is intended to prevent the flow of dc signals into the RF input port, which could result in damage to the signal source and introduce dc losses. The capacitor Cin has a limited effect on the rectifier input impedance and plays a minimal role in the matching process because of its small impedance value. Furthermore, the capacitor and inductor are modeled in accordance with Murata's 0402 package specifications. The dc output RL is 120 Ω. The diode utilized is the Schottky diode HSMS-270C, which is modeled after the datasheet. The rectifier circuit was simulated in ADS software, and the resulting simulation is shown in Figure 2b. From Figure 2b, it can be observed that the single sub-rectifier operates at 2.45 GHz; the rectifier efficiency of the left-pointing arrow is 70%, and Vout of the right-pointing arrow is 17 V when the input power is 35 dBm.

2.2. Design of a Power Divider

A 1 × 4 microstrip power divider is employed in this paper, which incorporates four sub-rectifier circuits to enhance the input power of the high-power rectifier. As previously stated, the maximum input power of a single sub-rectifier circuit is 35 dBm. Following connection of the power divider to four rectifier circuits, the input power is expanded to 35 dBm + 6 dB = 41 dBm, resulting in a 40 dBm high-power rectifier circuit with a 1 dB power margin reserved.

The 1 × 4 microstrip power divider described in this paper is constructed from three one-spart-two power dividers that have been spliced together. The design process of the one-spart-two microstrip power divider is presented next. As illustrated in Figure 3, the port 1 input impedance of the one-part-two power divider is 50 Ω, thus $Z_c = 50\,\Omega$. Given that it is an equal division power divider, the input impedance of the two parallel terminals satisfies Equation (9), and then one can compute $Z_A = Z_B = 100\,\Omega$. The two outputs of the microstrip line are $\lambda/4$ microstrip lines, and the load on the outputs is 50 Ω, thus

satisfying Equation (10), and then $Z_a = Z_b = 70.7\ \Omega$ can be computed, which completes the design of the one-part-two power divider. As illustrated in Figure 4a, the layout of three 1×2 power dividers have been integrated into a 1×4 power divider, and the size is 60.4 mm $\times$ 19.1 mm. The simulation outcomes in ADS are presented in Figure 4b. It can be observed that at the 2.45 GHz frequency point, the return loss S11 of the 1×4 power divider is indicated by the arrow pointing to the left, and S11 is -26.9 dB. The distribution loss S21 of the 1×4 power divider is indicated by the arrow pointing to the right, and S21 is -6.07 dB. In distribution loss S21, 0.07 dB of insertion loss is included. The 1×4 power divider meets design specifications.

$$\begin{cases} Z_A \parallel Z_B = Z_C = 50 \\ Z_A = Z_B \end{cases} \tag{9}$$

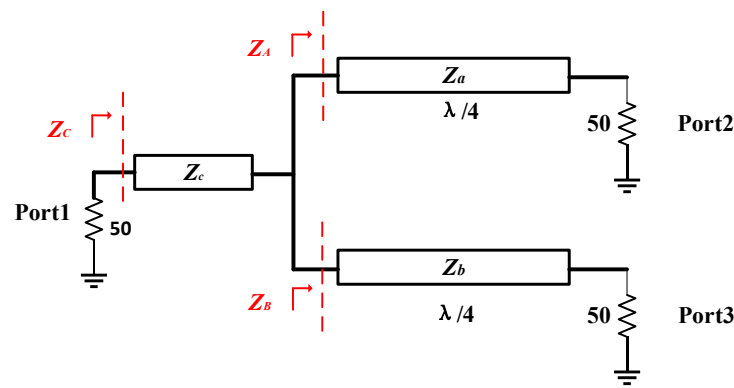$$\begin{cases} Z_A \times 50 = Z_a^2 \\ Z_B \times 50 = Z_b^2 \end{cases} \tag{10}$$

Figure 3. Schematic of the 1×2 power divider.
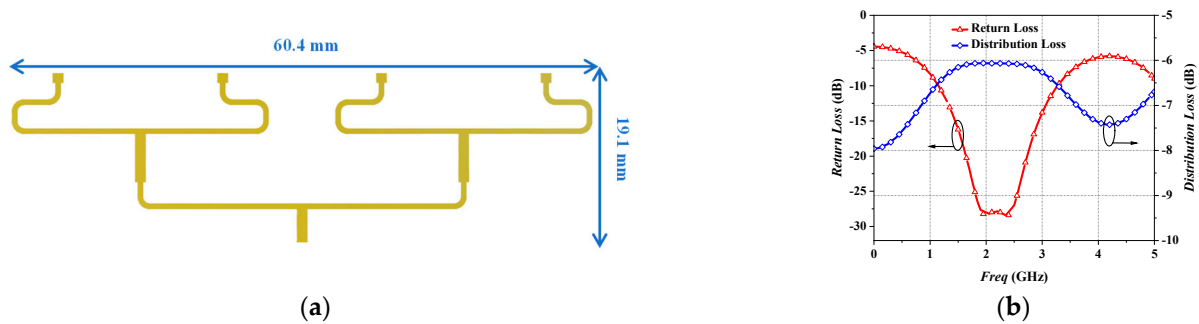

(**a**)　　　　　　　　　　　　　　　　　(**b**)

Figure 4. Proposed 1×4 power divider: (**a**) layout; (**b**) simulation of *S-Parameters* with *Freq*.

2.3. Design of Dc Synthesis

The conventional dc synthesis approach for rectifier circuits is typically a direct parallel synthesis (parallel-parallel), which is susceptible to high sensitivity to load variations. In this paper, first parallel and then series (parallel-series) dc synthesis is employed to enhance the rectifier circuit's resistance to load variations (load-carrying capacity) and the circuit's stability. As illustrated in Figure 5a, for the sake of simplicity, the four sub-rectifier circuits are equated to four dc sources, which are then connected to resistor loads for parallel-parallel and parallel-series dc synthesis, respectively. As illustrated in Figure 5b, two dc synthesis methodologies are simulated in ADS for a 10 W high-power rectifier circuit. For a rectifier efficiency exceeding 50%, the load of the parallel-parallel dc synthesis varies from 15 Ω to 75 Ω, with a load variation width of 60 Ω. The load variation range of parallel-series dc synthesis varies from 50 Ω to 325 Ω, with a load variation width of 275 Ω. This indicates that the load variation width of parallel-series dc synthesis is 215 Ω wider than parallel-parallel dc synthesis. Consequently, it can be concluded that parallel-series dc synthesis

has a stronger load-carrying capability. Accordingly, this paper employs parallel-serial dc synthesis to enhance the circuit's load-carrying capability and, consequently, its stability, as opposed to parallel-parallel dc synthesis.
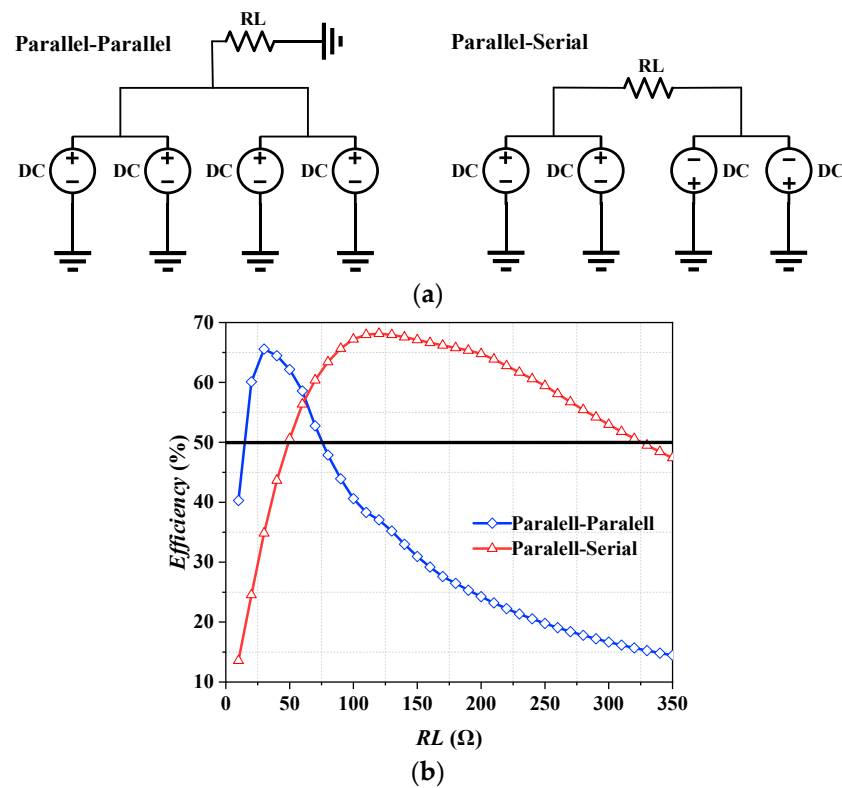

Figure 5. Parallel-parallel and parallel-series dc synthesis: (**a**) schematic; (**b**) simulation of *Efficiency* with *RL*.

3. Simulation and Measurement of a High-Power Rectifier

The four sub-rectifier circuits in Sections 2.1–2.3, a 1 × 4 power divider, and a parallel-series dc synthesizing network are combined to form a novel 10-Watt-Level high-power microwave rectifier circuit with a simple inverse Class-F harmonic network. A Rogers RO4003C, with a relative dielectric constant of 3.55, loss angle tangent of 0.0027, and thickness of 0.5 mm, was selected as the material for the board utilized in this rectifier circuit. The simulation design of this rectifier circuit was conducted using the industrial design software ADS. In this paper, the rectifier circuit is subjected to simulation, cast board processing, and measurement. The layout and physical diagram of the rectifier circuit are presented in Figure 6.

In contrast to the conventional approach of measuring low-power microwave rectifier circuits, the rectifier circuit cannot be directly connected to the signal source for measurement when measuring at high power. The high-power rectifier circuit, as illustrated in Figure 7, was connected to the framework in order to measure the aforementioned circuit. The Signal Generator (ROHDE&SCHWARZ SMN 100A) was utilized to generate 2.45 GHz microwave signals; the Circulator (UIYBCC3234A) was employed to isolate the reflex RF signal in order to prevent damage to the device. The PA (RFAMP–004060G-20W) was employed for the generation of high-power RF signals, which were utilized to drive the rectifier circuit. The Directional Coupler (SHWDCP-0506-30SFFF) was employed to couple the low-power signals to the spectrometer, which were utilized for rectifier input power measurements. The Spectrum Analyzer (KEYSIGHT CXA N9000A) was used for power measurements and readings. The Multimeter (KEYSIGHT 34465A) was used to read the voltage across the resistor load. Once the error value of the entire test apparatus had been compensated, the RF input power value of the rectifier circuit and the voltage value at

the two ends of the resistor load could be obtained, allowing the efficiency of the rectifier circuit to be calculated using Formula (11), and the variables of the formula are defined as follows:
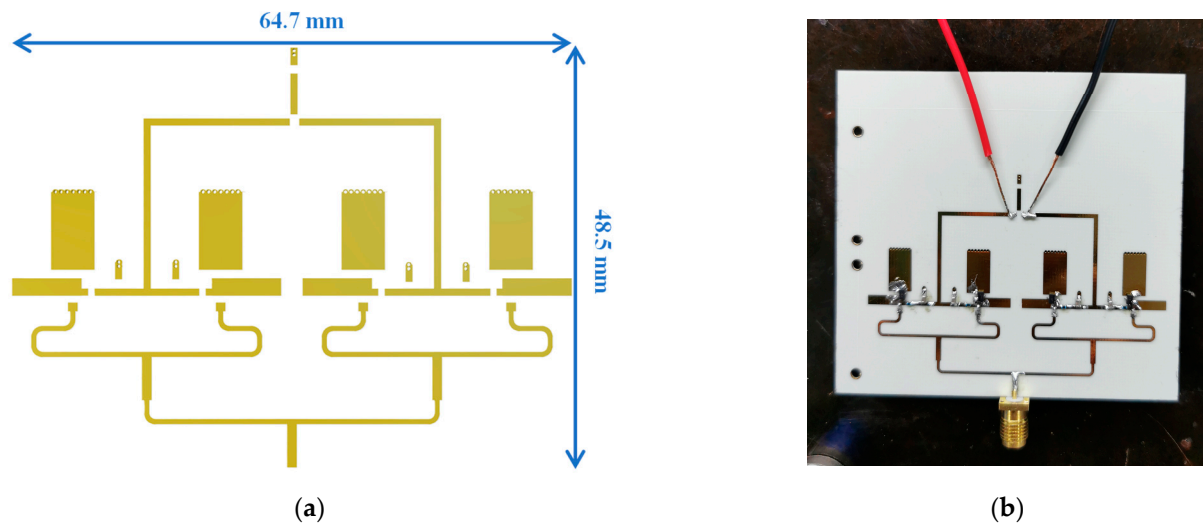
Figure 6. Proposed 10 W high-power rectifier: (**a**) layout; (**b**) fabricated circuit.
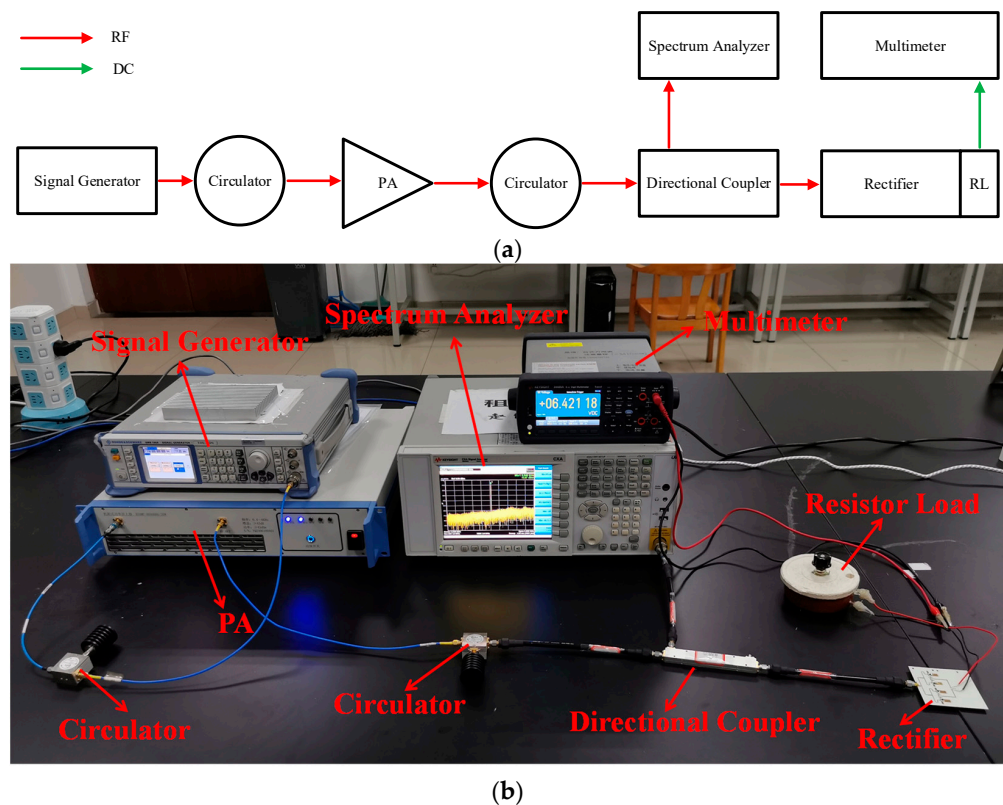
Figure 7. The measure environment of the high-power rectifier: (**a**) block diagram; (**b**) actual diagram.

Efficiency expresses the conversion efficiency of the rectifier.
Pout denotes the dc output power of the rectifier.
*Pin* signifies the microwave input power of the rectifier.
Vout represents the dc voltage across the resistor load.
RL is the resistor load.

$$Efficiency = \frac{Pout}{Pin} \times 100\% = \frac{Vout^2/RL}{Pin} \times 100\% \tag{11}$$

The simulated and measured curves of the 10 W Level inverse Class-F high power microwave rectifier circuit are presented in Figure 8. In the simulation, the maximum microwave input power is 41 dBm (12.45 W), with a rectifier efficiency of 66%, dc output power (*Pout*) of 8.2 W, dc output voltage (*Vout*) of 27.8 V, and *RL* of 94 Ω at an operating frequency of 2.45 GHz. The load variation range of simulation varies from 50 Ω to 325 Ω, with a load variation width of 275 Ω. In the measurements, the maximum microwave input power was observed to be up to 40 dBm (10 W), with a rectifier efficiency of 61.1%, dc output power (*Pout*) of 6.1 W, dc output voltage (*Vout*) of 23.9 V, and *RL* of 94 Ω. The input power from a 30 dBm (1 W) to 40 dBm (10 W) range of rectification efficiency is higher than 50% and has a large power range width. The load variation range of measurement varies from 50 Ω to 250 Ω, with a load variation width of 200 Ω. And the rectifier size is 64.7 mm × 48.5 mm. These results demonstrate that the expected high-power design has been achieved, and that the measurement aligns with the desired 10 W high-power design.
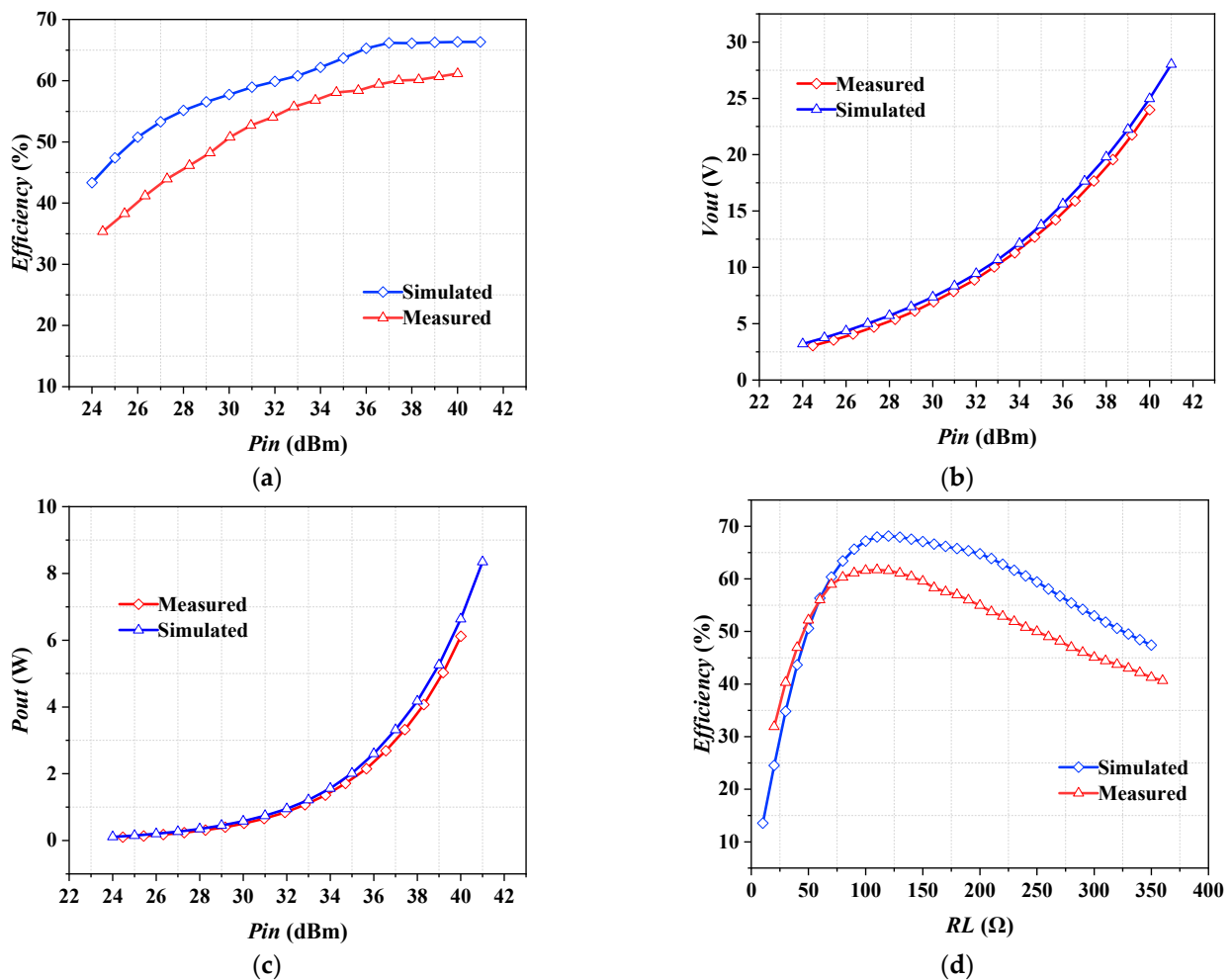
Figure 8. Simulation and measurement results: (**a**) *Efficiency-Pin*; (**b**) *Vout-Pin*; (**c**) *Pout-Pin*; (**d**) *Efficiency-RL*.

As illustrated in Figure 8, differences between the simulation data and the measured data remain evident in the performance curves of *Efficiency*, *Vout*, *Pout*, and *RL*. However, the overall differences are not significant. The differences between the simulation and measurement results can be attributed to the following factors: First and foremost, the ADS simulation of the diode equivalent circuit model is not sufficiently accurate relative to

actual diodes, resulting in different diode input impedances with the same input power and frequency. This ultimately gives rise to differences between the final simulation curve and the actual curve of the degree of conformity. Secondly, differences may also arise between the simulation model and the actual model due to the use of a Murata capacitor–inductor model in ADS. Additionally, differences may be observed between the same type of capacitor–inductor in different batches of production. These differences may contribute to a poor match between the simulation curve and the actual curve. Lastly, other secondary factors contribute to the differences between the simulation and measurement curves. These include soldering errors, SMA connector insertion loss compensation errors, temperature-related measurement errors, dielectric substrate parameter errors in actual production, and ADS simulation errors related to grounding hole setup, and so on. Collectively, these differences result in a poor match between the simulation and measurement curves.

As illustrated in Table 1, pertinent prior research is enumerated and evaluated. In regard to [24], it can be observed that a compact 5.8 GHz high-power rectifier circuit can be constructed with a single GaN Schottky diode, which is capable of attaining 71% rectification efficiency at an input power of 34 dBm. This represents an exemplary performance; however, it is regrettable that GaN Schottky diodes are not yet widely commercially available. In [15,25,26], a HSMS-280 series of silicon-based Schottky diodes were employed, resulting in a satisfactory input power and rectification efficiency. In [25,26], a four-cores HSMS-280P is employed to achieve rectification efficiencies of up to 79% at 30 dBm input power and 66.8% at 33 dBm input power, respectively. While the rectifier efficiencies of [25,26] are relatively high, their input powers remain insufficient in comparison to the present paper. In [30], the relatively uncommon four-core diode HSMS-270P is employed, with a single core voltage that is 10 V higher than that of the HSMS-280P. This indicates that the input power capacity of the HSMS-270P will exceed that of the HSMS-280P. The study in [30] achieves a rectification efficiency of 79% at 2.45 GHz with 38 dBm input power. The use of HSMS-270P to design a high-power rectifier represents a valuable approach that this paper should emulate. However, the maximum input power of this rectifier does not reach 40 dBm. In [31], the same method of a multiplexed power divider plus rectifier circuits is also used. When combined with a HSMS-2702 diode, this achieves a rectification efficiency of 62% at 41 dBm, thereby realizing a slightly greater input power and efficiency than this paper. However, the rectification efficiency in [31] operates at 0.92 GHz. Comparatively, the loss (including diode loss and dielectric substrate loss) incurred by operating at a higher frequency of 2.45 GHz in this paper becomes larger, which inherently causes a little decrease in the rectification efficiency.

Table 1. Comparison of rectifiers with high power.

Ref.	*Freq.* (GHz)	*Pin* (dBm)	*Eff.* (%)	*Vout* (V)	*RL* (Ω)	Size (mm^2)	Model	BV (V)
[24]	5.8	34	71	23.1	300	\	GaN	164
[25]	0.433	30	79	\	\	30 × 30	HSMS-282P	15
[26]	2.45	33	66.8	23	400	60 × 50	HSMS-282P	15
[15]	2.45	30	74.4	11.8	190	80 × 20	HSMS-2820	15
[30]	2.45	38	79	31.5	200	30 × 36	HSMS-270P	25
[31]	0.92	41	62	8.76	10	\	HSMS-2702	25
This work	2.45	40	61.1	23.9	94	64.7 × 48.5	HSMS-270C	25

4. Conclusions

A novel 10-Watt-Level high-power microwave rectifier with an inverse Class-F harmonic network for MPT is presented in this paper. The rectifier circuit is capable of realizing a high-power RF input of 40 dBm (10 W). Compared to existing technology, this paper's rectifier achieves a larger input power capacity than GaN-based diodes and other Si-based diodes by using the easy-to-purchase Si-based diode HSMS-270C. A 1 × 4 power divider, four sub-rectifier circuits with a simple inverse Class-F harmonic network, and a parallel-series dc synthesis network are used to form the high-power rectifier circuit. The RF power

distribution and parallel-series dc synthesis structure proposed in this paper represent a novel approach that not only extends RF power capacity but also increases the resistance variation range and enhances circuit stability. These were not considered in previous studies. The high-power rectifier circuit was measured at 2.45 GHz, achieving a maximum RF input power of 40 dBm (10 W), a peak rectifier efficiency of 61.1%, and an output DC voltage of 23.9 V. This high-power microwave rectifier circuit can be well applied in the MPT system to meet the demand of high-power energy transmission.

References

1.   Shoki, H. Issues and initiatives for practical use of wireless power transmission technologies in Japan. In Proceedings of the 2011 IEEE MTT-S International Microwave Workshop Series on Innovative Wireless Power Transmission: Technologies, Systems, and Applications, Kyoto, Japan, 12–13 May 2011; pp. 87–90. [CrossRef]

2.   Andrei, M.; Claudiu, B.; Vadan, I. Wireless Power Transmission—State of the Art and Applications. In Proceedings of the 2019 8th International Conference on Modern Power Systems (MPS), Cluj, Romania, 21–23 May 2019; pp. 1–6. [CrossRef]

3.   Li, J.L.W. Wireless power transmission: State-of-the-arts in technologies and potential applications (invited paper). In Proceedings of the Asia-Pacific Microwave Conference 2011, Melbourne, Australia, 5–8 December 2011; pp. 86–89.

4.   Dong, Y.; Dong, S.W.; Gao, S.; Wang, Y.; Li, X.; Wei, G. Design of Microwave Power Transmission System for Space Solar Power Station Demonstration. In Proceedings of the 2020 IEEE Wireless Power Transfer Conference (WPTC), Seoul, Republic of Korea, 15–19 November 2020; pp. 13–15. [CrossRef]

5.   Tanaka, K.; Kenichiro, M.; Takahashi, M.; Ishii, T.; Sasaki, S. Development of bread board model for microwave power transmission experiment from space to ground using small scientific satellite. In Proceedings of the 2012 IEEE MTT-S International Microwave Workshop Series on Innovative Wireless Power Transmission: Technologies, Systems, and Applications, Kyoto, Japan, 10–11 May 2012; pp. 191–194. [CrossRef]

6.   Shinohara, N. History and Innovation of Wireless Power Transfer via Microwaves. *IEEE J. Microw.* **2021**, *1*, 218–228. [CrossRef]

7.   Fuse, Y.; Saito, T.; Mihara, S.; Ijichi, K.; Namura, K.; Honma, Y.; Sasaki, T.; Ozawa, Y.; Fujiwara, E.; Fujiwara, T. Outline and progress of the Japanese microwave energy transmission program for SSPS. In Proceedings of the 2011 IEEE MTT-S International Microwave Workshop Series on Innovative Wireless Power Transmission: Technologies, Systems, and Applications, Kyoto, Japan, 12–13 May 2011; pp. 47–50. [CrossRef]

8.   Li, B.; Hu, B.-J.; Li, X.; Deng, M.; Wei, Z.-H. Efficiency enhancement of long-distance wireless power transmission using time reversal technique. In Proceedings of the 2016 IEEE International Conference on Computational Electromagnetics (ICCEM), Guangzhou, China, 23–25 February 2016; pp. 49–51. [CrossRef]

9.   Jiang, H.; Dou, W. Methods for Improving the Distance of Microwave Wireless Power Transmission with a Given Beam Collection Efficiency. *IEEE Antennas Wirel. Propag. Lett.* **2020**, *19*, 2112–2116. [CrossRef]

10. Kawasaki, S.; Kobayashi, Y.; Yoshida, S. High-power, high-efficiency microwave circuits and modules for wireless power transfer based on green-Eco technology. In Proceedings of the 2013 IEEE Radio and Wireless Symposium, Austin, TX, USA, 20–23 January 2013; pp. 28–30. [CrossRef]

11. Hu, L.; Ma, X.; Yang, G.; Zhang, Q.; Zhao, D.; Cao, W.; Wang, B.-Z. Auto-Tracking Time Reversal Wireless Power Transfer System with a Low-Profile Planar RF-Channel Cascaded Transmitter. *IEEE Trans. Ind. Electron.* **2023**, *70*, 4245–4255. [CrossRef]

12. Chaari, M.Z.; Al-maadeed, S. Wireless Power Transmission for the Internet of Things (IoT). In Proceedings of the 2020 IEEE International Conference on Informatics, IoT, and Enabling Technologies (ICIoT), Doha, Qatar, 2–5 February 2020; pp. 549–554. [CrossRef]

13. Halimi, M.A.; Khan, T.; Palandoken, M.; Kishk, A.A.; Antar, Y.M.M. Rectifier Design Challenges for Wireless Energy Harvesting/Wireless Power Transfer Systems: Broadening Bandwidth and Extended Input Power Range. *IEEE Microw. Mag.* **2023**, *24*, 54–67. [CrossRef]

14. Yu, X.; Lin, Y.-X.; Mitrovic, I.Z.; Hall, S.; Chao, D.-S.; Liang, J.-H.; Huang, Y.; Yen, T.-J.; Zhou, J. 900 MHz RF Power Rectifier Based on Ultra-low Turn-on Voltage Quasi-vertical GaN Schottky Diode. In Proceedings of the 2024 IEEE Wireless Power Technology Conference and Expo (WPTCE), Kyoto, Japan, 8–11 May 2024; pp. 441–444. [CrossRef]

15. Xiao, H.; Zhang, H.; Song, W.; Wang, J.; Chen, W.; Lu, M. A High-Input Power Rectifier Circuit for 2.45-GHz Microwave Wireless Power Transmission. *IEEE Trans. Ind. Electron.* **2022**, *69*, 2896–2903. [CrossRef]

16. Lai, S.; Zhang, Z.; Liu, Z.; Wang, G.; Zhou, Y.; Zhu, H.; Yang, Y. A Novel Self-Adaptive Rectifier with High Efficiency and Wide Input Power Range. *Electronics* **2023**, *12*, 712. [CrossRef]

17. Nguyen, D.-A.; Woo, K.; Bui, G.T.; Nam, H.; Seo, C. Wide Dynamic-Range and High-Efficiency Shunt-Diode Rectifier Based on Class-R Harmonic Control and Resistance Compression Network. *IEEE Trans. Circuits Syst. II Express Briefs* **2024**, *71*, 2359–2363. [CrossRef]

18. Chen, Y.-S.; Chiu, C.-W. Maximum Achievable Power Conversion Efficiency Obtained Through an Optimized Rectenna Structure for RF Energy Harvesting. *IEEE Trans. Antennas Propag.* **2017**, *65*, 2305–2317. [CrossRef]

19. Zeng, B.H.; Zheng, S.Y.; Leung, K.W.; Xia, M.H. An Ultrawideband High-Efficiency Rectifier Based on Harmonic Feedback Topology. *IEEE Trans. Ind. Electron.* **2022**, *69*, 7974–7983. [CrossRef]

20. Zhang, X.Y.; Du, Z.-X.; Xue, Q. High-Efficiency Broadband Rectifier with Wide Ranges of Input Power and Output Load Based on Branch-Line Coupler. *IEEE Trans. Circuits Syst. I Regul. Pap.* **2017**, *64*, 731–739. [CrossRef]

21. Yue, Z.; Xu, X.; Li, S.; Lin, X.Q.; Zhong, L.J.; Shi, M.D. Design of Efficient and Compact Ultrawideband Rectifier for Sub-6 GHz WPT/EH. *IEEE Microw. Wirel. Technol. Lett.* **2023**, *33*, 1490–1493. [CrossRef]

22. Huang, F.; Chu, C.; Zhang, Y.; Tian, K.; Jia, X.; Peng, H.; Zhang, Z.-H. GaN-based quasi-vertical Schottky barrier diodes with the sidewall field plate termination for obtaining low leakage current and high breakdown voltage. In Proceedings of the 2021 IEEE 1st International Power Electronics and Application Symposium (PEAS), Shanghai, China, 13–15 November 2021; pp. 1–4. [CrossRef]

23. Li, S.; Xu, X.; Kang, X.; Lan, J.; Yue, Z.; Zhao, R.; Wu, H.; Liu, X.; Lin, X. High-Efficiency and High-Power Rectifiers Using Cost-Effective AlGaN/GaN Schottky Diode with Accurate Large-Signal Parameter Extraction. *IEEE Microw. Wirel. Technol. Lett.* **2024**, *34*, 560–563. [CrossRef]

24. Dang, K.; Zhang, J.; Zhou, H.; Huang, S.; Zhang, T.; Bian, Z.; Zhang, Y.; Wang, X.; Zhao, S.; Wei, K.; et al. A 5.8-GHz High-Power and High-Efficiency Rectifier Circuit with Lateral GaN Schottky Diode for Wireless Power Transfer. *IEEE Trans. Power Electron.* **2020**, *35*, 2247–2252. [CrossRef]

25. Zhang, H.; Li, D.; Wang, Z.; Yang, L.; Shinohara, N.; Liu, Y. A Compact High-Efficiency Wideband Watt-Level RF Rectifier for Microwave Power Transfer. In Proceedings of the 2024 IEEE Wireless Power Technology Conference and Expo (WPTCE), Kyoto, Japan, 8–11 May 2024; pp. 445–448. [CrossRef]

26. Zhang, B.; Zhao, X.; Yu, C.; Huang, K.; Liu, C. A Power Enhanced High Efficiency 2.45 GHz Rectifier Based on Diode Array. *J. Electromagn. Waves Appl.* **2012**, *25*, 765–774. [CrossRef]

27. Young Yun, W.; Youngoo, Y.; Bumman, K. Analysis and experiments for high-efficiency class-F and inverse class-F power amplifiers. *IEEE Trans. Microw. Theory Tech.* **2006**, *54*, 1969–1974. [CrossRef]

28. Bui, G.T.; Nguyen, D.-A.; Seo, C. A Novel Design of Dual-Band Inverse Class-F Shunt-Diode Rectifier for Energy Harvesting. *IEEE Trans. Circuits Syst. II Express Briefs* **2023**, *70*, 2345–2349. [CrossRef]

29. Guo, J.; Zhang, H.; Zhu, X. Theoretical Analysis of RF-dc Conversion Efficiency for Class-F Rectifiers. *IEEE Trans. Microw. Theory Tech.* **2014**, *62*, 977–985. [CrossRef]

30. Xiao, H.; Song, W.; Chen, J.; Su, D.; Lu, W.; Zhang, H. An Impedance-Matching Voltage Regulator for High-Power Rectifier in Microwave Wireless Power Transmission. *IEEE J. Emerg. Sel. Top. Power Electron.* **2024**, *12*, 1173–1184. [CrossRef]

31. Liou, C.-Y.; Lee, M.-L.; Huang, S.-S.; Mao, S.-G. High-Power and High-Efficiency RF Rectifiers Using Series and Parallel Power-Dividing Networks and Their Applications to Wirelessly Powered Devices. *IEEE Trans. Microw. Theory Tech.* **2013**, *61*, 616–624. [CrossRef]